Coordination Chemistry

DOI: 10.1002/ange.201408649

The Mechanisms of Rectification in Au | Molecule | Au Devices Based on Langmuir–Blodgett Monolayers of Iron(III) and Copper(II) Surfactants**

*Lanka D. Wickramasinghe, Shivnath Mazumder, Sunalee Gonawala, Meeghage Madusanka Perera, Habib Baydoun, Bishnu Thapa, Li Li, Lingxiao Xie, Guangzhao Mao, Zhixian Zhou, H. Bernhard Schlegel, and Cláudio N. Verani**

Dedicated to Professor Robert Metzger on the occasion of his 75th birthday

Abstract: *Langmuir–Blodgett films of metallosurfactants were used in Au | molecule | Au devices to investigate the mechanisms of current rectification.*

In electronic circuitry, solid-state diodes enable current to flow in a given direction and prevent reversibility. This directional flow is defined as current rectification and is fundamental to the conversion of alternating into direct current necessary for information management. Molecular rectification—originally proposed by Aviram and Ratner[1] as a gedanken experiment—anticipates the feasibility of directional current flow in a molecule with well-defined donor and acceptor moieties. It was evaluated experimentally[2,3] in the early 1990s using an electrode–monolayer–electrode, E | LB | E, junction containing hexadecylquinolinium-tricyanoquinodimethane. The use of physisorbed Langmuir–Blodgett (LB) monolayers[4] prevents the formation of interfacial dipoles known as Schottky barriers typical of self-assembled systems, so that molecular rectification takes place either by asymmetric or unimolecular mechanisms that involve the frontier molecular orbitals (MOs) of the molecule. In asymmetric rectification, the lowest unoccupied LUMO of the acceptor in the molecule is energetically compatible with the Fermi levels of the electrodes, while the highest occupied HOMO is much lower in energy and does not participate in electron transfer (ET). On the other hand, in the unimolecular mechanism, the HOMO of the donor is equivalent in energy to the Fermi levels of an electrode, while the energy of the LUMO in the acceptor is equivalent to the second electrode.

Unimolecular rectification by organic systems has been reviewed in detail by Metzger et al.,[5–10] while the use of metal complexes has been considered to a lesser extent and predominantly on nickel and copper phthalocyanins.[11–14] The Yu group[15] studied a complex in which ruthenium(II) is coordinated to a thiophene-functionalized bipyridine and two fluorinated acetylacetonate (acac) groups. The rectification effect was explained by the presence of a permanent dipole moment perpendicular to the thiophene-functionalized bipyridine and along both acac ligands, being mediated through the HOMO, HOMO-3, and HOMO-4 orbitals associated with the t_{2g} set (d_{xy}, d_{yz}, d_{zx}) of the ruthenium(II) ion. We recently reported on the redox and electronic behavior of five-coordinate complexes where the iron(III) ion is bound to low-symmetry, phenolate-rich, $[N_2O_3]$ environments, and have shown that the molecular orbitals adapt their energies while the phenolate groups get oxidized.[16] These results served as base for another account[17] where an Au | LB | Au junction based on the alkoxylated iron(III) metallosurfactant $[Fe^{III}L^{N_2O_3}]$ acts as a molecular rectifier, with rectification ratios ($RR = [I$ at $-V_o / I$ at $+V_o]$) varying from 4.52 to 12 between -2 to $+2$ V and from 2.95 to 36.7 between -4 to $+4$ V.

In this report we evaluate the rectification response in two redox-responsive metallosurfactants aiming to correlate electronic structure and redox behavior with the mechanisms that determine molecular rectification in coordination complexes. These species are based on the new ligand $[H_2L^{N_2O_2}]$ and are the high-spin $3d^5$ $[Fe^{III}(L^{N_2O_2})Cl]$ (**1**) with an $S = 5/2$, sextet structure, and the $3d^9$ $[Cu^{II}(L^{N_2O_2})]$ (**2**), ($S = 1/2$, doublet) shown in Scheme 1.

The ligand $[H_2L^{N_2O_2}]$ was synthesized by reacting one equivalent of 4,5-bis(2-methoxyethoxy)benzene-1,2-diamine with two equivalents of 3,5-di-*tert*-butyl-2-hydroxybenzaldehyde under an inert atmosphere and reflux for 18 h and

[*] L. D. Wickramasinghe,[+] Dr. S. Mazumder,[+] S. Gonawala,[+] H. Baydoun, B. Thapa, Prof. H. B. Schlegel, Prof. C. N. Verani
Department of Chemistry, Wayne State University
5101 Cass Ave, Detroit, MI 48202 (USA)
E-mail: cnverani@chem.wayne.edu
Homepage: http://chem.wayne.edu/veranigroup/
M. M. Perera, Prof. Z. Zhou
Department of Physics & Astronomy, Wayne State University
666 W. Hancock, Detroit, MI 48201 (USA)
L. Li, L. Xie, Prof. G. Mao
Department of Chemical Engineering & Materials Science
Wayne State University
5050 Antony Wayne Dr., Detroit, MI 48202 (USA)
[+] These authors contributed equally to this work.

[**] The experimental portion of this work was funded by the National Science Foundation through the grants NSF-CHE1012413 to C.N.V., ECCS-1128297 to Z.Z., and CBET-0755654 to G.M., and include financial support for L.D.W. and S.G. The DFT calculations were funded by the U.S. Department of Energy, Office of Science, Basic Energy Sciences under the grant DE-SC0001907 to C.N.V. and H.B.S. and include financial support to S.M. Computer time allocated at the WSU—Grid System for the DFT is also acknowledged.

Supporting information for this article is available on the WWW under http://dx.doi.org/10.1002/anie.201408649.

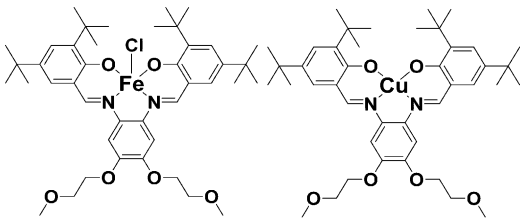

Scheme 1. The metallosurfactants.

includes electron donating *tert*-butyl groups and methoxyethoxy groups that modulate the redox, electronic, and amphiphilic properties of the resulting complexes. After recrystallization, $[H_2L^{N_2O_2}]$ was treated with one equivalent of the appropriate metal salt to yield complexes **1** and **2**. Synthetic schemes are shown in Scheme S1 in the Supporting Information. The IR spectroscopic data for **1** and **2** showed symmetric and asymmetric C–H stretching vibrations in the regions of 2820–2960 cm^{-1} and a prominent peak at 1585 cm^{-1} belonging to the C=N stretching vibrations. The high-resolution ESI-MS data showed $[M^+]$ at $m/z = 742.3641$ for **1** and $[M+H^+]$ at $m/z = 750.3661$ for **2** with isotopic patterns in good agreement with experimental and simulated data. The molecular structure of **2** was confirmed using X-ray crystal structure analysis (Figure 1, Table S2). It revealed the copper(II) complex in a square-planar geometry with an $[N_2O_2]$ environment where the nitrogen and oxygen atoms are trans to each other. The Cu–O and Cu–N distances are in agreement with reported values.[18,19]

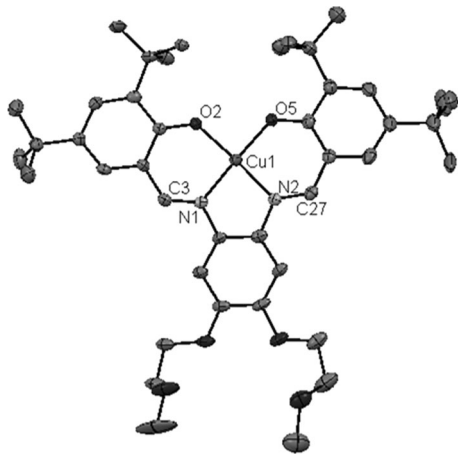

Figure 1. ORTEP representation at 50% probability for $[Cu^{II}(L^{N_2O_2})]$ (**2**). H atoms omitted for clarity.[54]

In order to access the nature of the frontier orbitals in **1** and **2**, electronic spectra were measured in 1.0×10^{-5} mol L^{-1} dichloromethane solutions (Figure S1, Table S3). Ligand-based $\pi\rightarrow\pi^*$ charge transitions were observed for $[H_2L^{N_2O_2}]$ between 280–360 nm. Species **1** showed bands at 310, 351, 395, and 447 nm with ε values ranging from 19200–49920 L mol^{-1} cm^{-1}. According to literature[20–22] and confirmed by time-dependent DFT (TD-DFT)[23–25] calculations along with the natural transition orbital (NTO) method,[26] bands at 310–400 nm are assigned as ligand-to-metal charge-transfer transitions (LMCT) from phenylenediamine- and phenolate-based p_π orbitals to d_{σ^*} and d_{π^*} iron(III)-based orbitals. The 447 nm band belong to intraligand $\pi\rightarrow\pi^*$ charge-transfer (ILCT) transitions[27] (Figure S2). Species **2** showed intense ILCT absorptions at 320, 349, 372, 419, 446, and a low intensity d-d band at 550 nm (Figure S1b). Four absorptions of reasonable oscillator strength have been found by TD-DFT calculations in the region of 318–462 nm (Figure S3). Therefore, the metal-based singly occupied SOMO is energetically and symmetry-wise more available in **1** than in **2**. The cyclic voltammograms of **1** and **2** (1.0×10^{-3} mol L^{-1}) were recorded versus the Fc^+/Fc couple and are shown in Figure 2.

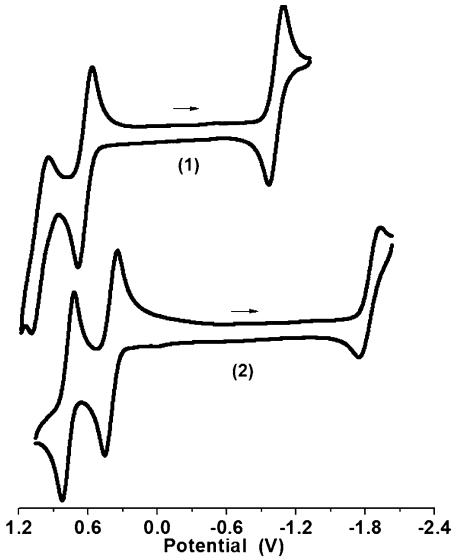

Figure 2. Cyclic voltammograms for **1** and **2**; DCM, vitreous C, Pt, Ag/AgCl, $TBAPF_6$. Potentials vs. the Fc^+/Fc couple.

Species **1** showed a quasi-reversible reduction at −1.02 V ($\Delta E_p = 0.12$ V, $|I_{pa}/I_{pc}| = 0.93$) assigned to the Fe^{III}/Fe^{II} redox couple, along with anodic processes at 0.64 V ($\Delta E_p = 0.12$ V, $|I_{pa}/I_{pc}| = 1.08$) and at 1.05 V ($\Delta E_p = 0.11$ V) attributed to ligand oxidations. Species **2** displayed two well-defined oxidation processes at 0.40 V ($\Delta E = 0.114$ V, $|I_{pa}/I_{pc}| = 1.1$) and 0.78 V ($\Delta E = 0.106$ V, $|I_{pa}/I_{pc}| = 1.0$) along with a quasi-reversible process at −1.85 V ($\Delta E = 0.192$ V, $|I_{pa}/I_{pc}| = 1.9$) attributed to the Cu^{II}/Cu^{I} reduction.[28] Spectroelectrochemical experiments (Figures S5 and S6) were revealing; the reduction of **1** into $\mathbf{1}^-$ at −1.38 $V_{Fc+/Fc}$ was accompanied by a decrease in the bands between 300–750 nm with a new band appearing at 451 nm, whereas the spectrum obtained for the reduction **2** to $\mathbf{2}^-$ at $V_{Fc+/Fc} = -2.07$ showed a decrease in all $\pi\rightarrow\pi^*$ transitions associated with the Cu^{II}/Cu^{I} couple. The first oxidation process for $\mathbf{1}^+$ at 0.88 and for $\mathbf{2}^+$ at $V_{Fc+/Fc} = 0.49$ showed an overall increase in intensity. Dominant features were observed at 1400 and 1100 nm respectively for $\mathbf{1}^+$ and $\mathbf{2}^+$ and attributed to ILCT $\pi\rightarrow\pi^*$ transitions. The electrochem-

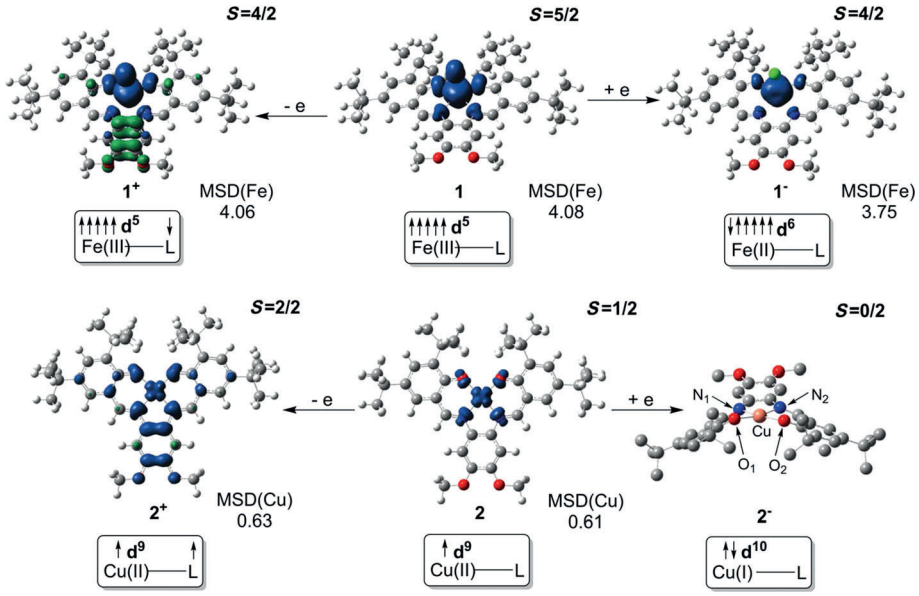

Figure 3. DFT-calculated spin density plots (isodensity 0.004 a.u.) showing oxidation and reduction for **1** and **2**. Hs omitted in $\mathbf{2}^{-}$.

ical events for **1** and **2** were further investigated using DFT methods.[29] Figure 3 shows spin densities for the relevant structures. The reduction of **1** was confirmed as an Fe^{III}/Fe^{II} event leading to the $^{HS}3d^6$ ($S=4/2$) iron(II) species $\mathbf{1}^{-}$ and associated with the observed disappearance of the $PhO^{-}\rightarrow Fe^{III}$ metal-to-ligand charge-transfer (MLCT) band.

The reduction of **2** is also confirmed as metal-centered and the resulting $3d^{10}$ copper(I) complex, $\mathbf{2}^{-}$, is a closed shell singlet ($S=0$) and severely distorted. The two phenoxyl rings are no longer coplanar leading to significant disruption of the π conjugation in the ligand framework responsible for the decrease in the ILCT processes observed in the spectroelectrochemical experiment. Therefore, we conclude that the metal reduction potentials corroborate with the spectroscopic results and confirm that the iron(III) SOMOs display lower energy than the copper(II) $d_{x^2-y^2}$ SOMO. On the other hand, the first oxidation to $\mathbf{1}^{+}$ is ligand-based yielding a radical delocalized over the phenylenediamine moiety. This π radical can couple antiferromagnetically (AF) with an electron from the singly occupied d_π orbital of iron producing an $S=4/2$ that is lower in energy than the counterpart ferromagnetically (F) coupled heptet ($S=6/2$) state by 3.7 kcal mol^{-1}. Oxidation of **2** is also found to be ligand-centered. In this case, the resulting phenylenediamine π-radical cannot couple with the copper-based singly occupied $d_{x^2-y^2}$ orbital and the HS triplet ($S=1$) state is found to be lower in energy than the AF coupled state ($S=0$) by 1.5 kcal mol^{-1}. The oxidation loci for $\mathbf{1}^{+}$ and $\mathbf{2}^{+}$ are different than the phenolate rings, as observed for the previously published rectifying $[N_2O_3]$ iron(III) complex,[17] but consistent with results presented by Thomas and co-workers.[18,19] The second oxidation for both $\mathbf{1}^{++}$ and $\mathbf{2}^{++}$ involves a phenolate to phenoxyl process, as illustrated in Figure S4.[30–32]

Metallosurfactants **1** and **2** form Langmuir (L) films, as measured by isothermal compression and Brewster angle microscopy (BAM; Figure S7). The surface pressure (π) vs. average molecular area (A) isotherm obtained for **1** showed an area of interaction of 74 Å^{2}molecule^{-1}, lacked acute phase transitions, and showed constant collapse pressure[33] around 40 mN m^{-1}, with a critical area of 71 Å^{2}molecule^{-1}. The BAM obtained during compression confirmed the formation of a homogeneous film from 9–38 mN m^{-1}. At 40 mN m^{-1} Newton rings were detected and associated with the collapse of the L film at the air/water interface.[34] Species **2** also showed good L-film formation with an area of interaction of 79 Å^{2}molecule^{-1} in spite of a lower collapse at 30 mN m^{-1}. BAM images reveal the formation of a homogenous film between 7–28 mN m^{-1}. Both films follow the Ries mechanism of collapse[35] discussed in other reported metallosurfactants.[36] Monolayers and multilayers were deposited onto glass, mica, and gold substrates at distinct surface pressures and analyzed by multiple methods. To probe the chemical integrity of the deposited molecules of **1** and **2**, the electronic spectra of 50-layer films on glass substrates were recorded. A comparison between film and solution spectra (Figure S8) shows that both species conserve the main original electronic processes, with minor decreased absorptions and red-shifting attributed to conformational changes associated with film packing[37] and J-type chromophore aggregation.[38,39] Infrared reflection absorption spectra (IRRAS) were also measured using *p*-polarized light at an angle of incidence of 30° for **1** and 40° for **2**,[40,41] and compared to the bulk IR spectra of **1** and **2** (Figure S9), showing equivalent peak patterning. Both species showed prominent bands belonging to $C{=}C_{(aromatic)}$ stretching and CH_n deformation vibration bands at 1610–1300 cm^{-1}, as well as pronounced C=N stretching at 1581 and 1587 cm^{-1} suggesting that the imine ligands remain intact after film deposition. Inference of film orientation by analysis of CH_2 vibration intensities[40–45] is limited because of the dominant contributions given by fourteen CH_3 groups present in both **1** and **2**. However, the CH_3 peak position in bulk and in the film shift from 2956 to 2964 cm^{-1} for **1** and 2954 to 2961 cm^{-1} for **2**, as expected in a well-packed film. Similarly, determination of molecular alignment angles for complex surfactants is elusive. However, contact angle measurements on the monolayers of structurally related species[17] indicate hydrophobic nature with the methoxyethoxy substituents attached to the glass substrate by van der Waals interactions and the *tert*-butyl groups oriented outwards. AFM measurements were carried out on LB monolayers deposited onto mica substrates at 15, 25, 30, 35, 37, and 40 mN m^{-1} for **1** and at 5, 10, 20, 25, 30, and 32 mN m^{-1} for **2** (Figures S10 and S11), with transfer ratios nearing unity. Monolayers of **1** deposited at

lower surface pressures showed random film organization and pin hole defects, while ordered and defect-free films were obtained at 30–35 mN m^{-1}. Homogeneous film formation for **2** was observed at 20–25 mN m^{-1}.

The LB monolayers transferred at surface pressures near collapse showed rougher surfaces with aggregate formation. Therefore, device fabrication used monolayers deposited onto gold-coated mica substrates at 35 and 25 mN m^{-1} for **1** and **2**, respectively, to minimize defects. The films were topped with a gold layer deposited using shadow masking.[6]

The resulting assemblies contained 16 Au | LB1 | Au and Au | LB2 | Au devices (Figure 4 inset) and had their rectification behavior probed as current–voltage (I/V) curves measured at ambient conditions. The reproducibility of the I/V characteristics were probed by measuring multiple devices of a given assembly, as well as by measuring different assemblies. An average of 25–30% of devices showed rectification in three assemblies. The data obtained for **1** and **2** are shown in Figure 4 and Figure S12.

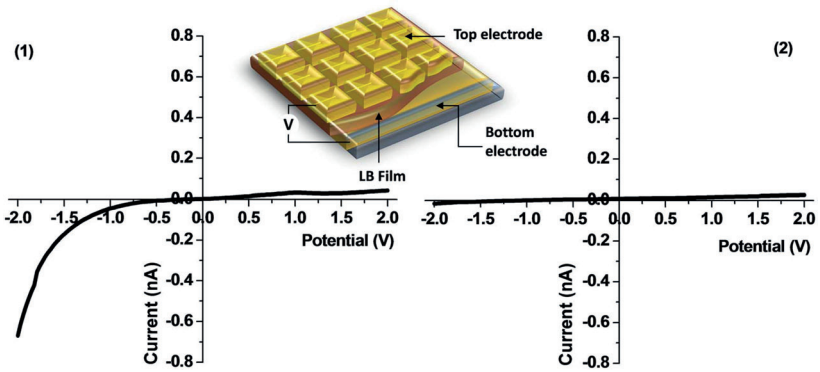

Figure 4. *I/V* characteristics observed for Au | LB1 | Au and Au | LB2 | Au. Inset: Representation of the assembly and individual devices.

Devices of Au | LB1 | Au showed asymmetric current response with elevated electrical current in the negative quadrant and negligible current response in the positive quadrant, as indicative of rectifying behavior (Figure S12 a–d). The observed rectification ratio (RR = [I at $-V_o$/I at $+V_o$])[46] ranges from 3.99 to 28.6 between -2 to $+2$ V and from 2.04 to 31 between -4 to $+4$ V. Reversing of the source and drain contacts reversed the I/V response, thus confirming the rectification behavior of **1** (Figures S12 e and S12 f). The amplitude of the forward current signal with reversed source and drain contacts is smaller, at around 0.3 nA, reflecting differences in molecular orientation of the film. Repeated measurement cycles led to a decrease in magnitude (Figure S12 b and S12 d) culminating in near-sigmoidal current responses (Figure S12 g). This behavior has been attributed to molecular reorientation to minimize the dipole moment and decrease the energy of a stable monolayer.[46] Remarkably, Au | LB2 | Au yielded flat I/V curves characteristic of non-rectifying devices.

Considering the distinctive behavior of **1** and **2**, an evaluation of the possible rectification mechanisms must take into account plausible ET pathways. As discussed previously, we reject a pure Schottky mechanism[6,8] because LB1 and LB2 are physisorbed by weak van der Walls interactions between two identical electrodes. However, we can suggest that the molecules are consistent with a [D-A] type structure, and that could support unimolecular mechanisms if the involved molecular orbitals display favorable energies. Nonetheless, these species lack an obvious HOMO/LUMO bridge to decrease electronic coupling, making this an unlikely mechanism of rectification.

The proposed model for ET through species in contact with metal electrodes requires that the Fermi levels (E_F) of the electrodes be compatible with the energies of the molecular frontier orbitals, when resonant tunneling can occur by different redox states of that given species. In gold electrodes E_F is 5.1 eV below vacuum,[47–49] and ET will be favored by the systems with the best match between E_F and HOMO/LUMO or HOMO/SOMO (singly occupied) energies. Therefore, we need to consider the redox behavior of the metallosurfactants, knowing that the difference between the first oxidation potential (E_{pa1}) and the first reduction potential (E_{pc1}) is roughly equivalent to the energy of the HOMO–LUMO gap. The iron(III) species **1** displayed a smaller ΔE ($= E_{pa1} - E_{pc1}$) of 1.78 V when compared to that of the copper(II) species **2** given by $\Delta E = 2.39$ V, suggesting a narrower HOMO–LUMO energy gap for **1**. The molecular redox potentials measured from cyclic voltammetric experiments, can be converted to comparable solid-state potentials using the following equations, $V_a = 4.7\ \text{eV} + E_{1/2}^{red}(\text{SCE})$ and $V_i = 4.7\ \text{eV} + (1.7)E_{1/2}^{ox}(\text{SCE})$, where V_a and V_i are very close to the first electron affinity and first ionization energy levels of the molecule supported on the electrodes, respectively.[50–53] The $E_{1/2}^{red}(\text{SCE})$ and $E_{1/2}^{ox}(\text{SCE})_{1/2}$ values are the measured half-wave first reduction and first oxidation potentials at -0.61 and 1.05 V for complex **1**, respectively, and -1.46 and 0.79 V for complex **2**, referenced versus the saturated calomel electrode (SCE).

Using these values, the V_a energy of the first metal-centered SOMO is calculated to be -4.1 eV for **1** and -3.2 eV for **2**, respectively. Similarly, the V_i energy equivalent to the first ligand-centered HOMOs are found to be -6.5 and -6.1 eV for **1** and **2**, respectively. Therefore, the model depicted in Figure 5, shows that the gold Fermi levels are approximately 1.0 eV below the lowest energy Fe-based SOMO of species **1**. Because of the asymmetry of the molecule, this SOMO is a linear combination described as $d_{xz} + d_{yz}$, when the molecular z axis is maintained along the Fe–Cl direction. Electrode-to-molecule ET is likely to occur when a bias is applied triggering the population of that orbital—which corresponds to the generation of an iron(II) center—and subsequent lowering of the energy of the resulting doubly occupied MO. On the other hand, the only available SOMO for **2** is the copper-based $d_{x^2-y^2}$ orbital that lies approximately 2 eV above the electrode Fermi level. This MO is likely not attainable at the applied bias, and this

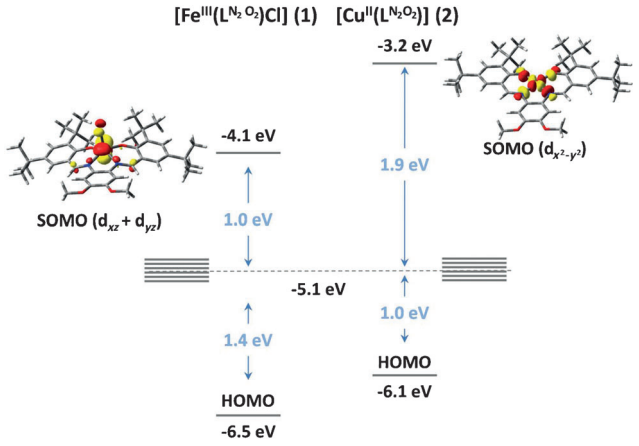

Figure 5. Electron transfer model involving the Fermi levels of the electrode into the metal-based SOMOs of **1** and **2**.

energetic mismatch accounts for the observed *I*/*V* non-rectifying behavior of the copper(II) complex. The gap of 1.4 eV between E_F and V_i for **1** suggests that the ligand-based HOMOs are not involved in the rectification process, whereas the difference between E_F and V_i for **2** is comparable to that between E_F and V_a for **1**. As no rectification has been observed for the copper(II) species, it indicates that the molecule-to-electrode ET cannot be the determining step. Thus, considering 1) the rectifying behavior for **1** along with the appropriate energy match between E_F and V_a and the possible mismatch between E_F and V_i, and 2) the non-rectifying behavior of **2** where the difference between E_F and V_a is large and E_F and V_i is small, an asymmetric current rectifying mechanism is tentatively proposed. Additionally, local orbital asymmetry might also play a role; while the $d_{x^2-y^2}$-based SOMO of the non-rectifying **2** is described as D_{2h}, the ($d_{xz} + d_{yz}$)-based SOMO of the rectifying **1** displays an idealized C_s symmetry. This aspect is being explored in further detail.

In summary, we have successfully compared the behavior of new iron(III) and copper(II) surfactants **1** and **2** towards current rectification. The lowest metal-centered SOMO in **1** seems energetically affordable for electrode-to-molecule ET, and an asymmetric rectification mechanism is suggested. Thus, a generalization can be proposed that metallosurfactants in defect-free monolayers might exhibit rectification properties if available SOMOs display energies similar to those of the Fermi levels of gold electrodes. Molecular geometry, electronic configurations, and local symmetries will further determine which SOMO is energetically favorable.

Received: August 28, 2014
Revised: September 18, 2014
Published online: November 3, 2014

Keywords: coordination chemistry · current rectification · device fabrication · electron transfer · molecular rectification

[1] A. Aviram, M. Ratner, *Chem. Phys. Lett.* **1974**, *29*, 277 – 283.
[2] A. S. Martin, J. R. Sambles, G. J. Ashwell, *Phys. Rev. Lett.* **1993**, *70*, 218 – 221.
[3] G. J. Ashwell, J. R. Sambles, A. S. Martin, W. G. Parker, M. Szablewski, *J. Chem. Soc. Chem. Commun.* **1990**, 1374 – 1376.
[4] K. Ariga, Y. Yamauchi, T. Mori, J. P. Hill, *Adv. Mater.* **2013**, *25*, 6477 – 6512.
[5] W. J. Shumate, D. L. Mattern, A. Jaiswal, D. A. Dixon, T. R. White, J. Burgess, A. Honciuc, R. M. Metzger, *J. Phys. Chem. B* **2006**, *110*, 11146 – 11159.
[6] R. M. Metzger, *J. Mater. Chem.* **2008**, *18*, 4364 – 4396.
[7] R. M. Metzger, *Chem. Rec.* **2004**, *4*, 291 – 304.
[8] R. M. Metzger, *Chem. Rev.* **2003**, *103*, 3803 – 3834.
[9] C. Krzeminski, C. Delerue, G. Allan, D. Vuillaume, R. M. Metzger, *Phys. Rev. B* **2001**, *64*, 085405.
[10] R. M. Metzger, *Acc. Chem. Res.* **1999**, *32*, 950 – 957.
[11] W. J. Pietro, *Adv. Mater.* **1994**, *6*, 239 – 242.
[12] S. Roth, S. Blumentritt, M. Burghard, C. M. Fischer, G. Philipp, C.-M. Schwanneke, *Synth. Met.* **1997**, *86*, 2415 – 2418.
[13] M. H. Yoon, A. Facchetti, T. J. Marks, *Proc. Natl. Acad. Sci. USA* **2005**, *102*, 4678 – 4682.
[14] G. J. Ashwell, B. Urasinska, W. D. Tyrrell, *Phys. Chem. Chem. Phys.* **2006**, *8*, 3314 – 3319.
[15] Y. Lee, S. Yuan, A. Sanchez, L. Yu, *Chem. Commun.* **2008**, 247 – 249.
[16] M. M. Allard, J. A. Sonk, M. J. Heeg, B. R. McGarvey, H. B. Schlegel, C. N. Verani, *Angew. Chem. Int. Ed.* **2012**, *51*, 3178 – 3182; *Angew. Chem.* **2012**, *124*, 3232 – 3236.
[17] L. D. Wickramasinghe, M. M. Perera, L. Li, G. Mao, Z. Zhou, C. N. Verani, *Angew. Chem. Int. Ed.* **2013**, *52*, 13346 – 13350; *Angew. Chem.* **2013**, *125*, 13588 – 13592.
[18] A. Kochem, O. Jarjayes, B. Baptiste, C. Philouze, H. Vezin, K. Tsukidate, F. Tani, M. Orio, Y. Shimazaki, F. Thomas, *Chem. Eur. J.* **2012**, *18*, 1068 – 1072.
[19] M. Orio, O. Jarjayes, H. Kanso, C. Philouze, F. Neese, F. Thomas, *Angew. Chem. Int. Ed.* **2010**, *49*, 4989 – 4992; *Angew. Chem.* **2010**, *122*, 5109 – 5112.
[20] B. P. Gaber, V. Miskowski, T. G. Spiro, *J. Am. Chem. Soc.* **1974**, *96*, 6868 – 6873.
[21] R. Mayilmurugan, E. Suresh, M. Palaniandavar, *Inorg. Chem.* **2007**, *46*, 6038 – 6049.
[22] M. Velusamy, M. Palaniandavar, S. R. Gopalan, G. U. Kulkarni, *Inorg. Chem.* **2003**, *42*, 8283 – 8293.
[23] L. Petit, P. Maldivi, C. Adamo, *J. Chem. Theory Comput.* **2005**, *1*, 953 – 962.
[24] E. Runge, E. K. U. Gross, *Phys. Rev. Lett.* **1984**, *52*, 997 – 1000.
[25] R. E. Stratmann, G. E. Scuseria, M. J. Frisch, *J. Chem. Phys.* **1998**, *109*, 8218 – 8224.
[26] R. L. Martin, *J. Chem. Phys.* **2003**, *118*, 4775 – 4777.
[27] O. Rotthaus, O. Jarjayes, C. Philouze, C. P. D. Valle, F. Thomas, *Dalton Trans.* **2009**, 1792 – 1800.
[28] H. Arora, C. Philouze, O. Jarjayes, F. Thomas, *Dalton Trans.* **2010**, *39*, 10088 – 10098.
[29] R. G. Parr, W. Yang, *Density-functional theory of atoms and molecules*, Oxford University Press, New York, **1989**.
[30] M. Lanznaster, H. P. Hratchian, M. J. Heeg, L. M. Hryhorczuk, B. R. McGarvey, H. B. Schlegel, C. N. Verani, *Inorg. Chem.* **2006**, *45*, 955 – 957.
[31] F. D. Lesh, R. Shanmugam, M. M. Allard, M. Lanznaster, M. J. Heeg, M. T. Rodgers, J. M. Shearer, C. N. Verani, *Inorg. Chem.* **2010**, *49*, 7226 – 7228.
[32] R. C. Pratt, L. M. Mirica, T. D. P. Stack, *Inorg. Chem.* **2004**, *43*, 8030 – 8039.
[33] S. Kundu, A. Datta, S. Hazra, *Langmuir* **2005**, *21*, 5894 – 5900.
[34] J. Galvan-Miyoshi, S. Ramos, J. Ruiz-Garcia, R. Castillo, *J. Chem. Phys.* **2001**, *115*, 8178 – 8184.
[35] H. E. Ries, Jr., *Nature* **1979**, *281*, 287 – 289.

[36] R. Shakya, S. S. Hindo, L. Wu, M. M. Allard, M. J. Heeg, H. P. Hratchian, B. R. McGarvey, S. R. P. da Rocha, C. N. Verani, *Inorg. Chem.* **2007**, *46*, 9808 – 9818.
[37] A. Dhanabalan, S. V. Mello, O. N. Oliveira, Jr., *Macromolecules* **1998**, *31*, 1827 – 1832.
[38] H. Menzel, J. S. McBride, B. Weichart, M. Ruther, *Thin Solid Films* **1996**, *284 – 285*, 640 – 643.
[39] H. Menzel, B. Weichart, A. Schmidt, S. Paul, W. Knoll, J. Stumpe, T. Fischer, *Langmuir* **1994**, *10*, 1926 – 1933.
[40] G. Brezesinski, B. Dobner, C. Stefaniu, D. Vollhardt, *J. Phys. Chem. C* **2011**, *115*, 8206 – 8213.
[41] L. Wang, A. Cruz, C. R. Flach, J. Pérez-Gil, R. Mendelsohn, *Langmuir* **2007**, *23*, 4950 – 4958.
[42] S. Joy, P. Pal, T. K. Mondal, G. B. Talapatra, S. Goswami, *Chem. Eur. J.* **2012**, *18*, 1761 – 1771.
[43] G. Brezesinski, B. Dobner, C. Stefaniu, D. Vollhardt, *Langmuir* **2011**, *27*, 5386 – 5392.
[44] J. Kattner, H. Hoffmann, *External reflection spectroscopy of thin films on dielectric substrates: Hand book of vibrational spectroscopy*, Wiley, Chichester, **2002**, pp. 12 – 14.
[45] T. Hasegawa, J. Umemura, T. Takenaka, *J. Phys. Chem.* **1993**, *97*, 9009 – 9012.
[46] R. M. Metzger, B. Chen, U. Hopfner, M. V. Lakshmikantham, D. Vuillaume, T. Kawai, X. Wu, H. Tachibana, T. V. Hughes, H. Sakurai, J. W. Baldwin, C. Hosch, M. P. Cava, L. Brehmer, G. J. Ashwell, *J. Am. Chem. Soc.* **1997**, *119*, 10455 – 10466.
[47] L. Zhang, J. A. Bain, J. G. Zhu, L. Abelmann, T. Onoue, *IEEE Trans. Magn.* **2004**, *40*, 2549 – 2551.
[48] K. Kitagawa, T. Morita, S. Kimura, *Langmuir* **2005**, *21*, 10624 – 10631.
[49] K. Seo, A. V. Konchenko, J. Lee, G. S. Bang, H. Lee, *J. Am. Chem. Soc.* **2008**, *130*, 2553 – 2559.
[50] J. He, Q. Fu, S. Lindsay, J. W. Ciszek, J. M. Tour, *J. Am. Chem. Soc.* **2006**, *128*, 14828 – 14835.
[51] "Scanning Tunneling Spectroscopy": K. W. Hipps in *Handbook of Applied Solid State Spectroscopy* (Ed.: D. R. Vij), Springer, Berlin, **2006**, chap. 7.
[52] L. Scudiero, D. E. Barlow, K. W. Hipps, *J. Phys. Chem. B* **2002**, *106*, 996 – 1003.
[53] A. Schmidt, N. R. Armstrong, C. Goeltner, K. Muellen, *J. Phys. Chem.* **1994**, *98*, 11780 – 11785.
[54] CCDC 1024931 (2) contains the supplementary crystallographic data for this paper. These data can be obtained free of charge from The Cambridge Crystallographic Data Centre via www.ccdc.cam.ac.uk/data_request/cif. See also the Supporting Section for the crystal data.

